Hidden charge density wave induced shadow bands and ultrafast dynamics of CuTe investigated using time-resolved ARPES

Haoyuan Zhong [●],[1] Changhua Bao [●],[1] Tianyun Lin [●],[1] Fei Wang [●],[1] Xuanxi Cai [●],[1] Pu Yu,[1,2] and Shuyun Zhou [●][1,2,*]

[1]*State Key Laboratory of Low-Dimensional Quantum Physics and Department of Physics, Tsinghua University,*
Beijing 100084, People's Republic of China
[2]*Frontier Science Center for Quantum Information, Beijing 100084, People's Republic of China*

Revealing the fine electronic structure is critical for understanding the underlying physics of low-dimensional materials. Angle-resolved photoemission spectroscopy (ARPES) is a powerful experimental technique for mapping out the experimental electronic structure. By reducing the photon energy (e.g., to 6 eV) using laser sources, a greatly improved momentum resolution can be achieved, thereby providing opportunities for "zooming in" the fine electronic structure and even revealing the previously unresolvable bands near the Brillouin zone center. Here, by using quasi-one-dimensional material CuTe as an example, we demonstrate the unique capability of laser-based ARPES in revealing the fine electronic structures of "hidden" charge density wave induced shadow bands near the Brillouin zone center, which are previously unresolvable using synchrotron light sources. The observation of the shadow bands reveals the CDW phase from the aspect of band folding, and the unpredicted CDW band hybridization strongly modifies the electronic structure and Fermi surface, which suggests that such hybridization must be taken into account for studying the CDW transition. Moreover, the ultrafast nonequilibrium carrier dynamics are captured by time-resolved ARPES, revealing the relaxation dynamics through electron-phonon scattering. Our work demonstrates the advantages of laser-based ARPES in zooming in the fine electronic structures, as well as capturing the ultrafast dynamics of low-dimensional materials.

I. INTRODUCTION

The electronic structure $E(k)$ determines the physical properties of low-dimensional materials, and therefore experimentally mapping out their electronic structure is critical. Angle-resolved photoemission spectroscopy (ARPES) is a powerful experimental technique for probing the electronic structure $E(k)$ of low-dimensional materials [1–3]. Figure 1(a) shows a schematic experimental setup for ARPES, where a probe light source excites electrons from the solid-state materials. The range of accessible in-plane momentum $k_\parallel = 0.512 \cdot \sin\theta\sqrt{h\nu - E_B - \phi}$ is determined by the photon energy $h\nu$, where θ is the emission angle, E_B is the binding energy of photoelectrons, and ϕ is the work function. In order to cover a large energy and momentum range, synchrotron light sources with a photon energy of 20–100 eV are often used, which, however, also inevitably leads to a compromised in-plane momentum resolution $\Delta k_\parallel = 0.512 \cdot \cos\theta\sqrt{h\nu - E_B - \phi} \cdot \Delta\theta$. Reducing the photon energy from 100 eV to $\sim$ 6 eV using laser sources [4–13] can significantly improve $\Delta k_\parallel$ by almost eight times [Fig. 1(b)], making low energy laser-ARPES a potential "microscope" [see schematic illustration in Fig. 1(c)] for zooming in the fine electronic structures near the Brillouin zone (BZ) center, which are otherwise not resolvable using higher photon energy light sources generated from synchrotrons. In addition, the ultrafast laser

pulses also allow to capture the ultrafast carrier dynamics after exciting the sample with a pump beam by performing ARPES measurements in the pump-probe scheme, namely time-resolved ARPES (TrARPES) [14–22].

Here, we demonstrate the advantages of laser-ARPES in revealing the fine electronic structures near the BZ center of various quantum materials, such as Li-intercalated graphene, topological semimetal $PtSn_4$, and charge density wave (CDW) materials $IrTe_2$ and CuTe. Using CuTe as an example [23–25], we further show that the "hidden" CDW shadow bands, which were unresolvable in previous ARPES measurements using synchrotron light sources [24], can now be clearly resolved using $\sim$6 eV laser sources, and the CDW-induced band hybridization is identified below the CDW transition temperature. Moreover, by performing TrARPES with a pump pulse, the relaxation dynamics of photoexcited carriers are captured, revealing the role of electron-phonon (el-ph) scattering in nonequilibrium state. Our work provides insights into the CDW physics of CuTe, and demonstrates the advantages of low energy laser-ARPES in zooming in the fine electronic structures near the BZ center as well as revealing the related nonequilibrium carrier dynamics.

II. RESULTS AND DISCUSSION

Low-energy laser-ARPES can not only "magnify" the electronic structures near the BZ center, more interestingly it can reveal the previously unresolvable "hidden" bands [7,13] as demonstrated in Figs. 1(d)–1(k). Figure 1(d) shows the
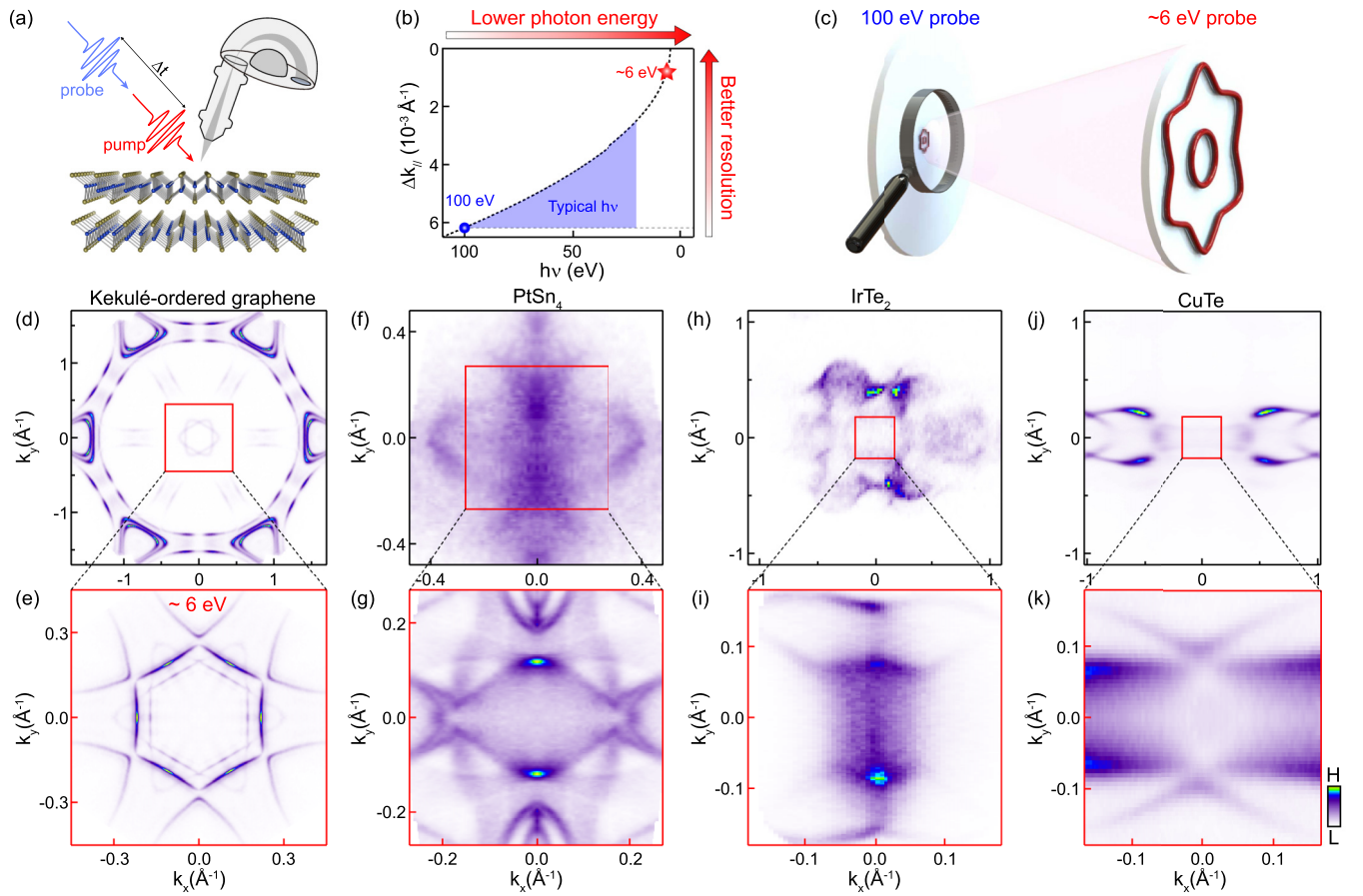
FIG. 1. Zooming in the fine electronic structures by laser ARPES. (a) Schematics of laser-based TrARPES setup. (b) The momentum resolution as a function of photon energy. The work function ϕ is 4.5 eV, θ is 45°, and $\Delta\theta$ is 0.1° in calculations. (c) Schematics of the "microscope" ability of zooming in Fermi surface structures of laser ARPES. (d) and (e) Fermi surface of Kekulé-ordered graphene measured by the (d) helium lamp source at $h\nu = 21.2$ eV and the (e) laser source with $h\nu = 6.2$ eV at 80 K. (f) and (g) Fermi surface map of $PtSn_4$ measured by the (f) helium lamp source with $h\nu = 21.2$ eV and (g) laser source (symmetrized with respect to k_x and $k_y = 0$) with $h\nu = 6.7$ eV at 80 K. (h) and (i) Fermi surface map of $IrTe_2$ measured by the (h) synchrotron source with $h\nu = 100$ eV and the (i) laser source with $h\nu = 6.2$ eV at 80 K [28]. (j) and (k) Fermi surface map of CuTe measured by the (j) synchrotron source with $h\nu = 80$ eV at 20 K [24] and the (k) laser source with $h\nu = 6.3$ eV at 80 K.

Fermi surface map of Li-intercalated graphene where the pockets near the K points are folded to the Γ point by the $(\sqrt{3} \times \sqrt{3})$R30° Kekulé order [26,27]. While the three pockets corresponding to trilayer graphene are clearly observed near the BZ corners using the helium lamp source, only one set of replica pockets is observed near the Γ point [26,29]. Laser-ARPES measurements instead can zoom in the fine electronic structures near the BZ center, and resolve the other two folded pockets as shown in Fig. 1(e). In topological semimetal $PtSn_4$, which has a complex Fermi surface structure [30,31], only some broad features are observed in the Fermi surface map in Fig. 1(f) using a helium lamp source. Interestingly, laser-ARPES measurements successfully resolve a nice and complex fine electronic structure in Fig. 1(g). For CDW materials, the shadow bands induced by band folding due to the CDW periodicity are typically much weaker than the original bands, which are therefore often "hidden" or unresolvable as compared to the strong original bands. Laser-ARPES measurements provide new opportunities for resolving such "hidden" shadow bands. Figures 1(h)–1(k) show comparisons between the Fermi surface maps measured

with high and low photon energies in two CDW materials, $IrTe_2$ [28,32,33] and CuTe [24], where CDW-induced shadow bands are clearly resolved as shown in Figs. 1(i) and 1(k), demonstrating the power of laser-ARPES measurements in magnifying the "hidden" shadow bands. Moreover, the probe laser source with tunable photon energy provides opportunities for overcoming the dipole element effects, which either enhance or suppress the intensity of the bands (see Fig. S1 in the Supplemental Material [34]). The four types of materials presented above demonstrate that laser-ARPES measurements can provide opportunities for zooming in the fine electronic structures, and even revealing the previously unresolvable bands of quantum materials near the Γ point. Especially for CuTe, revealing the "hidden" shadow bands helps to understand the CDW state from another aspect (folded bands due to new lattice periodicity), complementary to the aspect of the CDW energy gap [24]. Therefore, below we further use CuTe as an example to explore the physics of the "hidden" bands, including evidence of band folding and CDW-induced hybridization gaps, as well as the ultrafast dynamics.
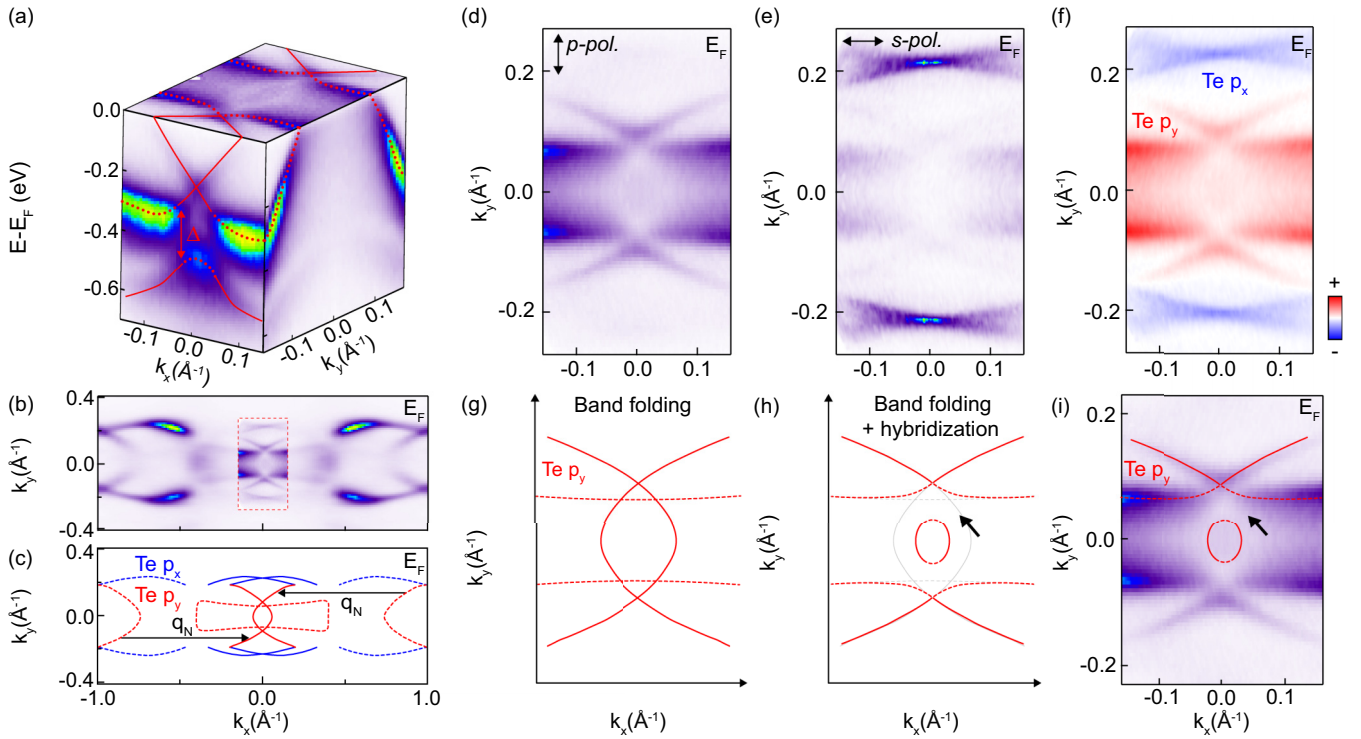
FIG. 2. Revealing the "hidden" CDW shadow bands by laser ARPES. (a) Three-dimensional electronic structure of CuTe by laser ARPES. (b) Fermi surface map of CuTe measured using a high photon energy ($h\nu = 80$ eV). The inset is the sum of the laser-ARPES data measured at $h\nu = 6.3$ eV with s and p polarizations. (c) Schematics of Fermi surface of CuTe due to CDW-induced band folding. Red and blue curves represent Te p_y and p_x contributions [24]. Dashed curves are the original pockets while solid curves are replicas translated by the CDW vectors. (d) and (e) Fermi surface maps using p-pol. and s-pol. respectively (symmetrized with respect to $k_y = 0$), and the directions of the electrical field are marked by the arrows. (f) Differential intensity by subtracting (e) from (d). (g) and (h) Schematic of replica pockets without (g) and with (h) band hybridization. The band hybridization between the original pockets and folded pockets opens up a gap at the crossing points. (i) Fermi surface map with the schematic in (h) over plotted.

CuTe is a quasi-one-dimensional room-temperature CDW material [23], whose CDW band structure has been investigated by synchrotron-based ARPES measurements [24], while CDW-induced shadow bands remain elusive. The successful observation of CDW shadow bands by laser ARPES allows to investigate the CDW phase transition of CuTe from a new perspective, namely the evolution of the shadow bands. Figure 2(a) shows the full three-dimensional electronic structure of CuTe using laser ARPES. To further confirm that the observed new bands near the Γ point are from CDW shadow bands, we compare the fine Fermi surface map (marked by red dashed box) with a large-ranged Fermi surface map measured by a high photon energy in Fig. 2(b). As schematically summarized in Fig. 2(c), the CDW nesting vectors $q_x = \pm 0.4a^*$ [24] translate the pockets (dashed curves) originated from Te p_x (blue) and p_y (red) orbitals near the BZ boundary to the Γ point, and the replica pockets (solid curves) match well with the measured Fermi surface by laser ARPES, thereby suggesting that they are likely shadow bands induced by the CDW order.

Polarization-dependent laser-ARPES measurements are performed to further confirm the symmetry properties of these shadow bands. Figures 2(d) and 2(e) show a comparison of the Fermi surface maps using two different light polarizations: p-pol., where the electric field is along the k_y direction; and s-pol., where the electric field is along the k_x direction.

Distinct intensity distributions are observed, and the differential (dichroic) intensity spectrum is shown in Fig. 2(f). The polarization-dependent laser-ARPES measurements show that the pockets around Γ (red) and away from Γ (blue) are from Te p_y and p_x, respectively (similar to the polarization-dependent ARPES measurements in another p orbital system [38]), which are also consistent with the symmetry properties of the original bands [24]. However, the simple band folding picture in Fig. 2(g) does not fully match the measured Fermi surface map shown in Fig. 2(i), suggesting there is significant hybridization between the shadow bands (red solid curves) and original bands (red dashed curves), as schematically illustrated in Fig. 2(h). Such hybridization also results in the gap opening in Fig. 2(a).

The CDW phase transition can be directly visualized by tracing the evolution of the shadow bands and the hybridization gap with temperature. As shown in Figs. 3(a)–3(f), the shadow bands marked by red arrows gradually disappear with increasing temperature, and eventually become undetectable at 320 K, which is near the CDW phase transition temperature. Similar temperature evolution is also observed in the dispersion images shown in Figs. 3(g)–3(l). Moreover, the hybridization gap [indicated by the blue arrow in Fig. 3(g)] also decreases gradually with increasing temperature. The electronic structure without hybridization is schematically shown in Fig. 3(m), where hybridization between shadow and origin
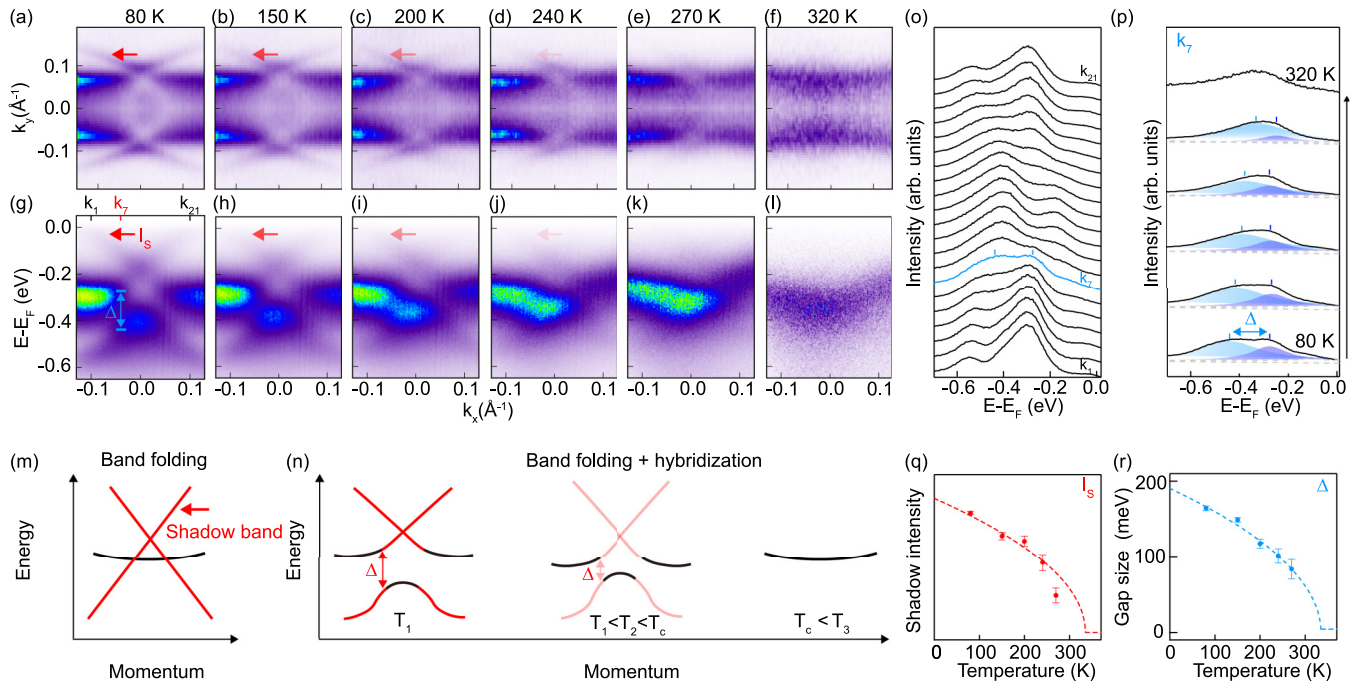
FIG. 3. Temperature dependence of CDW folding and hybridization. (a)–(f) Fermi surface maps with temperature ranging from 80 K to 320 K (symmetrized with respect to $k_y = 0$). (g)–(l) Corresponding dispersion images along $k_y = 0.12$ Å^{-1} in (a), where the I_S is the intensity of the shadow bands and Δ is the hybridization gap. (m) Schematic of the electronic structure without hybridization. (n) Schematic summary of CDW melting when increasing the temperature: decreasing of hybridization gap and weakening of shadow band. (o) Extracted EDCs from k_1 to k_{21} marked in (g). (p) Extracted EDCs at momentum position k_7 in (o) from 80 K to 320 K, which are fitted by three Lorentzian peaks and the main peaks are filled blue. (q) Extracted shadow band intensity I_S (see Fig. S2 for raw data in the Supplemental Material [34]), the red dashed line is the BCS-type gap equation with transition temperature $T_c = 335$ K. (r) Extracted gap size from (p) as a function of temperature, the blue dashed line is the BCS-type gap equation with transition temperature $T_c = 335$ K. We note that the gap is hardly distinguished at 320 K due to the broad bandwidth.

bands opens up a hybridization gap. With increasing temperature, both the shadow band intensity and the hybridization gap decrease when approaching the CDW phase transition as shown in Fig. 3(n). A quantitative analysis of the shadow band intensity is shown in Supplemental Material Fig. S2 [34], and analysis of the hybridization gap is performed by fitting the energy distribution curves (EDCs) measured at the momentum k_7 [the blue curve in Fig. 3(o)] with different temperatures as shown in Fig. 3(p). The evolution of the shadow band intensity [Fig. 3(q)] and the hybridization gap [Fig. 3(r)] is consistent with the BCS-type gap equation [24,39,40], suggesting that the weakening of shadow bands and the decreasing of the hybridization gap are both induced by the suppression of the CDW order. The unpredicted band hybridization between the shadow bands and original bands not only opens hybridization gaps but also strongly modifies the "topology" of the Fermi surface which should have impact on its physical properties (e.g., transport properties). Such an observation demonstrates the important role of band hybridization between shadow bands and original bands in CDW transition, which has been, however, largely ignored in previous studies. Our new finding suggests that such hybridization must be taken into account for studying the CDW transition in the future. The observation of CDW-induced shadow bands and hybridization gap, made possible by low-energy laser-ARPES measurements, provides new

perspectives for the electronic structure modification of CuTe in the CDW phase.

The ultrafast probe laser pulses have another advantage: the capability to measure the ultrafast carrier dynamics by combining a pump beam in TrARPES measurements. Meanwhile, revealing the ultrafast dynamics is important for CDW materials [16,18,41,42], because electron-phonon (el-ph) and electron-electron (el-el) scattering can drive the relaxation dynamics. We first investigate the electronic structure evolution of CuTe upon photoexcitation. Figures 4(a)–4(e) show TrARPES snapshots of CuTe at different delay times, where the representative delay times are marked in the time trace [integrating red box in Fig. 4(c)] in Fig. 4(f). The photoexcited electronic states can be better revealed in the differential images in Figs. 4(g)–4(j), which are obtained by subtracting the dispersion image by data measured at −1 ps. A fast relaxation dynamics is clearly distinguished by comparing data at 0.2 ps [Fig. 4(h)] and 0.6 ps [Fig. 4(i)], which is quantitatively analyzed in Fig. 5.

The energy and momentum resolved carrier dynamics is further revealed, which helps us to distinguish the relaxation dynamics. The energy and momentum dependent temporal evolution is shown in Figs. 5(b) and 5(c), which is extracted from energies and momentums marked in Fig. 5(a). For all energies and momentums, the relaxation dynamics lies between 200–600 fs, which are obtained by fitting the temporal
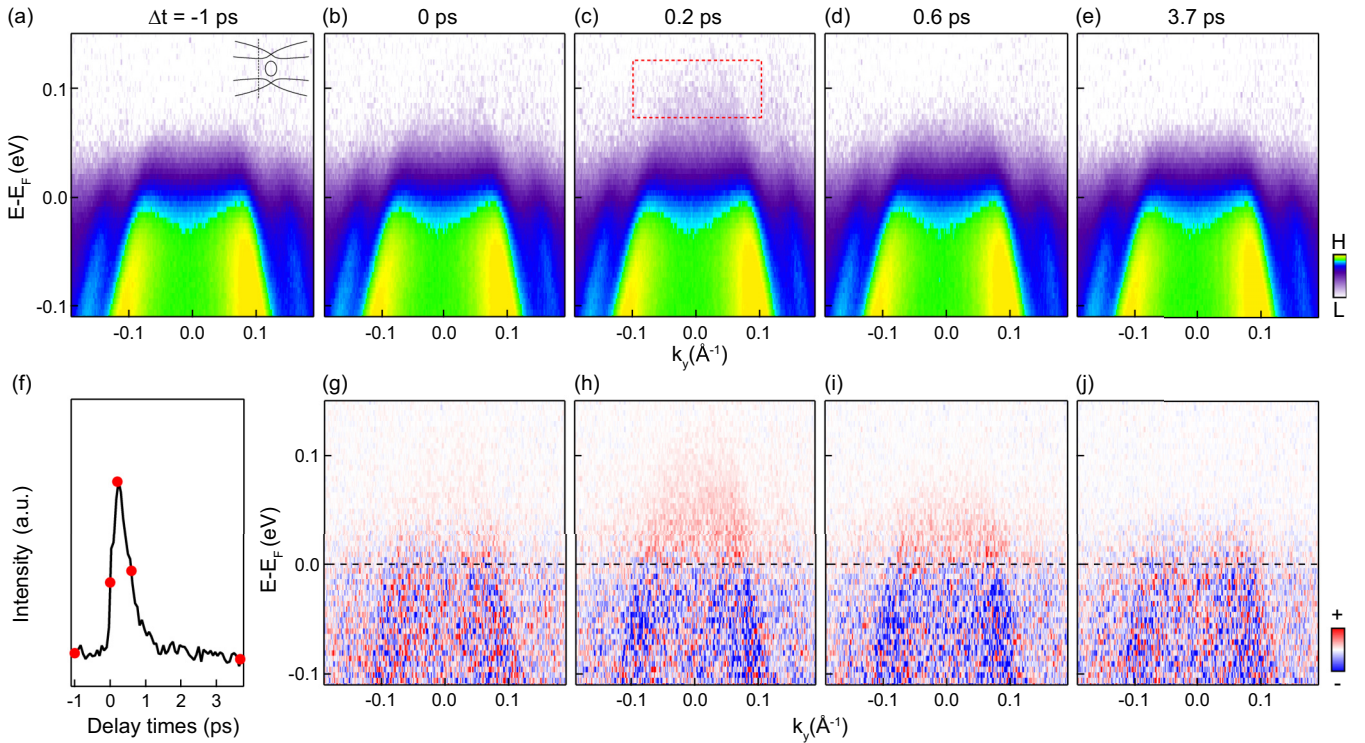
FIG. 4. Transient electronic structure of CuTe upon photoexcitation. (a)–(e) Snapshots of electronic dispersion (dispersion along k_x = -0.08 Å^{-1} illustrated in the inset) at different pump-probe delay times marked in (f). (f) Temporal evolution of photoexcited electrons integrated by the red dashed box in (c). (g)–(j) Differential TrARPES spectra at different delay times after subtracting the spectrum at −1 ps. The pump and probe photon energies are 1.58 eV and 6.3 eV, respectively, with a pump fluence of 280 μJ/cm^2 measured at 80 K.

evolution of the ARPES intensity [46]. Here, we further analyze the energy-dependent lifetime τ [from Fig. 5(b)] and scattering rate $1/\tau$, which are plotted in Fig. 5(d). The lifetime is consistent with the recent complimentary reflectivity measurements of the same material [47]. Such relaxation time is much faster compared to many quantum materials, for example, Bi$_2$Se$_3$ [17,48] and Cd$_3$As$_2$ [49], which might indicate strong el-ph coupling (inversely proportional to relaxation times [49,50]) in CuTe, as theoretical calculations [24,51–53] and transport measurement [54] indicated. We note that the el-ph coupling induced kink feature is not resolvable in our measurements, which is not surprising considering that the phonon energy is quite low, ∼10 meV, smaller than the energy resolution of 46 meV (see Fig. S3 for energy resolution in Supplemental Material [34]). In addition to the carrier dynamics, the photoexcited thermodynamics can also be revealed. Figure 5(e) shows the continuous evolution of EDCs as a function of delay times by integrating momentum range Δk_1 in Fig. 5(a), where the transient electronic temperature is extracted by fitting the EDCs with a Fermi-Dirac distribution, as shown in Fig. 5(f). The evolution of the electronic temperature T_e shows a relaxation time of 470 ± 70 fs as shown in Fig. 5(g) near the Γ point [Δk_1 in Fig. 5(a)] and a relaxation time of 510 ± 60 fs as shown in Fig. 5(h) away from the Γ point [Δk_2 in Fig. 5(a)], which are both ∼500 fs. First, compared to the characteristic time scale, which is 10–100 fs for el-el scattering and is 100–1000 fs for el-ph scattering [18], we can infer that photocarriers of CuTe relax through el-ph scattering. Second, relaxation timescale of CuTe is com-

parable to many CDW materials, for example, TbTe$_3$ [16], 1T-TaS$_2$ [55,56], 1T-TiSe$_2$ [41], and 1T-TaSe$_2$ [42] (all of them relax with time scale of a few hundred of femtoseconds). While those CDW materials relax through el-ph scattering, we indicate that the relaxation dynamics of CuTe is driven by el-ph scattering. We would like to note that el-el scattering (supported by calculation [24]) cannot be fully ruled out since the timescale of tens of femtoseconds might not be distinguished.

III. CONCLUSION

In summary, by using laser-ARPES with low photon energy, a significantly improved momentum resolution is achieved, allowing to successfully reveal the fine electronic structures near the Γ point for various quantum materials. Using CuTe as an example, the CDW phase transition is revealed from the view of "hidden" shadow bands. Interestingly, the unpredicted CDW band hybridization strongly modifies the electronic structure and Fermi surface, which suggests that such hybridization must be taken into account for the physics of the CDW transition. Moreover, the ultrafast nonequilibrium carrier dynamics are captured by time-resolved ARPES, revealing the relaxation dynamics through el-ph scattering. Our work demonstrates the power of low energy laser ARPES in zooming in the fine electronic structures and ultrafast dynamics near the BZ center, which can be extended to a wide range of quantum materials.
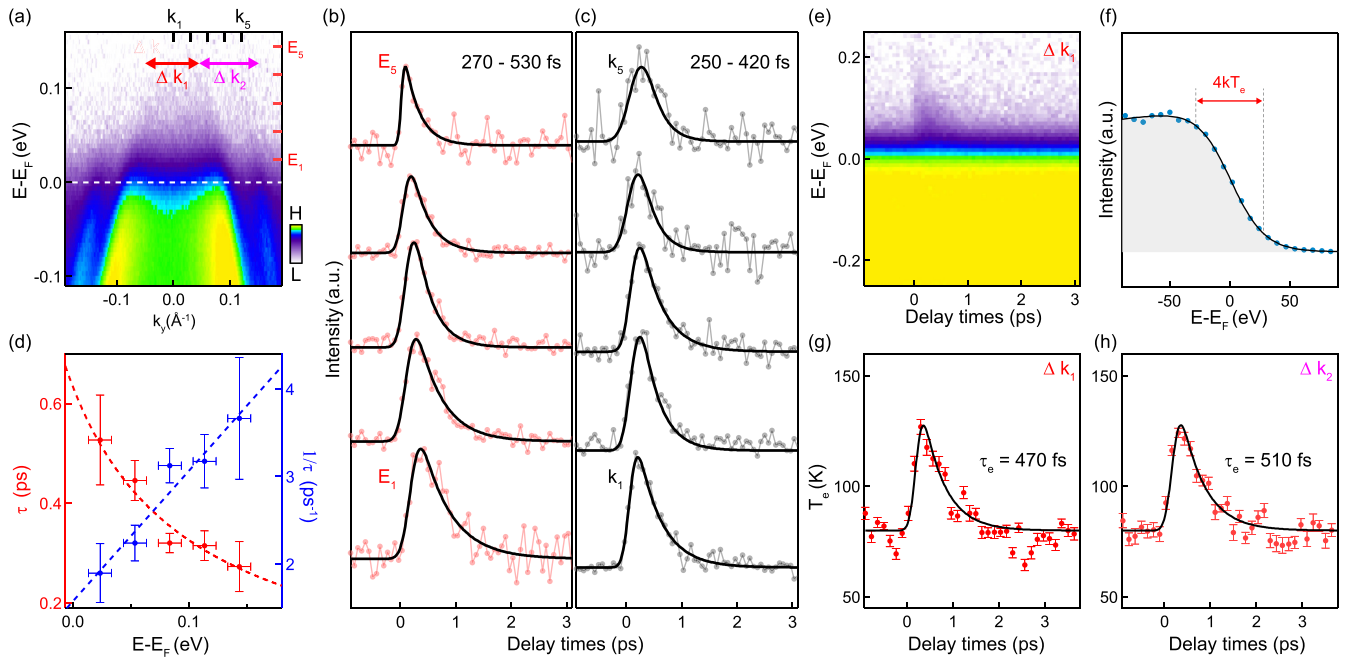
FIG. 5. Ultrafast relaxation dynamics of CuTe upon photoexcitation. (a) Snapshot of electronic structure (along $k_x = -0.08$ Å^{-1}) at pump-probe delay time $\Delta t = 0.2$ ps. (b) Temporal evolution of photoexcited electrons at a few selected energies (integrate momentum range of -0.05–0.05 Å) indicated by red tick marks E_1–E_5 in (a). (c) Temporal evolution of photo-excited electrons at a few selected momentums (integrate energy range of 0.05–0.15 eV) indicated by black tick marks k_1–k_5 in (a). (d) Extracted lifetime τ (red) and scattering rate $1/\tau$ (blue) of photoexcited electrons as a function of energy, where $1/\tau$ is fitted by a line. (e) Integrated EDCs at momentum range Δk_1 marked in (a) as a function of delay time. (f) EDC at delay time of -500 fs from (e) and corresponding Fermi-Dirac fitting. (g), (h) Extracted electronic temperature as a function of delay time (g) near the Γ point [Δk_1 in(a)] and (h) away from the Γ point [Δk_2 in(a)]. Note that the electronic temperature increase in CuTe is low, similar to the case in metal [43–45], which is due to high electron density of state near the Fermi level. The pump and probe photon energies are 1.58 eV and 6.3 eV, respectively, with a pump fluence of 280 μJ/cm^2 measured at 80 K. Time resolution and energy resolution are shown in Fig. S3 in the Supplemental Material [34].

[1] A. Damascelli, Z. Hussain, and Z.-X. Shen, Rev. Mod. Phys. **75**, 473 (2003).

[2] J. A. Sobota, Y. He, and Z.-X. Shen, Rev. Mod. Phys. **93**, 025006 (2021).

[3] H. Zhang, T. Pincelli, C. Jozwiak, T. Kondo, R. Ernstorfer, T. Sato, and S. Zhou, Nat. Rev. Methods Primers **2**, 54 (2022).

[4] J. D. Koralek, J. F. Douglas, N. C. Plumb, Z. Sun, A. V. Fedorov, M. M. Murnane, H. C. Kapteyn, S. T. Cundiff, Y. Aiura, K. Oka *et al.*, Phys. Rev. Lett. **96**, 017005 (2006).

[5] T. Kiss, T. Shimojima, K. Ishizaka, A. Chainani, T. Togashi, T. Kanai, X.-Y. Wang, C.-T. Chen, S. Watanabe, and S. Shin, Rev. Sci. Instrum. **79**, 023106 (2008).

[6] G. Liu, G. Wang, Y. Zhu, H. Zhang, G. Zhang, X. Wang, Y. Zhou, W. Zhang, H. Liu, L. Zhao *et al.*, Rev. Sci. Instrum. **79**, 023105 (2008).

[7] J. Meng, G. Liu, W. Zhang, L. Zhao, H. Liu, X. Jia, D. Mu, S. Liu, X. Dong, J. Zhang *et al.*, Nature (London) **462**, 335 (2009).

[8] K. Deng, G. Wan, P. Deng, K. Zhang, S. Ding, E. Wang, M. Yan, H. Huang, H. Zhang, Z. Xu *et al.*, Nat. Phys. **12**, 1105 (2016).

[9] A. Tamai, Q. S. Wu, I. Cucchi, F. Y. Bruno, S. Riccò, T. K. Kim, M. Hoesch, C. Barreteau, E. Giannini, C. Besnard *et al.*, Phys. Rev. X **6**, 031021 (2016).

[10] F. Y. Bruno, A. Tamai, Q. S. Wu, I. Cucchi, C. Barreteau, A. De la Torre, S. McKeownWalker, S. Riccò, Z. Wang, T. K. Kim *et al.*, Phys. Rev. B **94**, 121112(R) (2016).

[11] C. Bareille, S. Suzuki, M. Nakayama, K. Kuroda, A. H. Nevidomskyy, Y. Matsumoto, S. Nakatsuji, T. Kondo, and S. Shin, Phys. Rev. B **97**, 045112 (2018).

[12] C. Lin, M. Ochi, R. Noguchi, K. Kuroda, M. Sakoda, A. Nomura, M. Tsubota, P. Zhang, C. Bareille, K. Kurokawa *et al.*, Nat. Mater. **20**, 1093 (2021).

[13] S. Kunisada, S. Isono, Y. Kohama, S. Sakai, C. Bareille, S. Sakuragi, R. Noguchi, K. Kurokawa, K. Kuroda, Y. Ishida *et al.*, Science **369**, 833 (2020).

[14] F. Boschini, M. Zonno, and A. Damascelli, Rev. Mod. Phys. **96**, 015003 (2024).

[15] L. Perfetti, P. A. Loukakos, M. Lisowski, U. Bovensiepen, H. Eisaki, and M. Wolf, Phys. Rev. Lett. **99**, 197001 (2007).

[16] F. Schmitt, P. S. Kirchmann, U. Bovensiepen, R. G. Moore, L. Rettig, M. Krenz, J.-H. Chu, N. Ru, L. Perfetti, D. H. Lu *et al.*, Science **321**, 1649 (2008).

[17] J. A. Sobota, S. Yang, J. G. Analytis, Y. L. Chen, I. R. Fisher, P. S. Kirchmann, and Z.-X. Shen, Phys. Rev. Lett. **108**, 117403 (2012).

[18] S. Hellmann, T. Rohwer, M. Kalläne, K. Hanff, C. Sohrt, A. Stange, A. Carr, M. Murnane, H. Kapteyn, L. Kipp *et al.*, Nat. Commun. **3**, 1069 (2012).

[19] S. Gerber, S.-L. Yang, D. Zhu, H. Soifer, J. A. Sobota, S. Rebec, J. J. Lee, T. Jia, B. Moritz, C. Jia *et al.*, Science **357**, 71 (2017).

[20] S.-L. Yang, J. A. Sobota, Y. He, D. Leuenberger, H. Soifer, H. Eisaki, P. S. Kirchmann, and Z.-X. Shen, Phys. Rev. Lett. **122**, 176403 (2019).

[21] C. Bao, P. Tang, D. Sun, and S. Zhou, Nat. Rev. Phys. **4**, 33 (2022).

[22] S. Ulstrup, A. G. abo, J. A. Miwa, J. M. Riley, S. S. Grønborg, J. C. Johannsen, C. Cacho, O. Alexander, R. T. Chapman, E. Springate *et al.*, ACS Nano **10**, 6315 (2016).

[23] K. Stolze, A. Isaeva, F. Nitsche, U. Burkhardt, H. Lichte, D. Wolf, and T. Doert, Angew. Chem. Int. Ed. **52**, 862 (2013).

[24] K. Zhang, X. Liu, H. Zhang, K. Deng, M. Yan, W. Yao, M. Zheng, E. F. Schwier, K. Shimada, J. D. Denlinger *et al.*, Phys. Rev. Lett. **121**, 206402 (2018).

[25] S. Kwon, H. Jung, S. Lee, G. Y. Cho, K. Kong, C. Won, S.-W. Cheong, and H. W. Yeom, Nat. Commun. **15**, 984 (2024).

[26] C. Bao, H. Zhang, T. Zhang, X. Wu, L. Luo, S. Zhou, Q. Li, Y. Hou, W. Yao, L. Liu *et al.*, Phys. Rev. Lett. **126**, 206804 (2021).

[27] C. Bao, H. Zhang, X. Wu, S. Zhou, Q. Li, P. Yu, J. Li, W. Duan, and S. Zhou, Phys. Rev. B **105**, L161106 (2022).

[28] C. Bao, H. Zhang, Q. Li, S. Zhou, H. Zhang, K. Deng, K. Zhang, L. Luo, W. Yao, C. Chen *et al.*, Commun. Phys. **4**, 229 (2021).

[29] H. Zhang, C. Bao, M. Schüler, S. Zhou, Q. Li, L. Luo, W. Yao, Z. Wang, T. P. Devereaux, and S. Zhou, Natl. Sci. Rev. **9**, nwab175 (2022).

[30] E. Mun, H. Ko, G. J. Miller, G. D. Samolyuk, S. L. Bud'ko, and P. C. Canfield, Phys. Rev. B **85**, 035135 (2012).

[31] Y. Wu, L.-L. Wang, E. Mun, D. D. Johnson, D. Mou, L. Huang, Y. Lee, S. L. Budko, P. C. Canfield, and A. Kaminski, Nat. Phys. **12**, 667 (2016).

[32] T. Qian, H. Miao, Z. Wang, X. Shi, Y. Huang, P. Zhang, N. Xu, L. Zeng, J. Ma, P. Richard *et al.*, New J. Phys. **16**, 123038 (2014).

[33] K. Kim, S. Kim, K.-T. Ko, H. Lee, J.-H. Park, J. J. Yang, S.-W. Cheong, and B. I. Min, Phys. Rev. Lett. **114**, 136401 (2015).

[34] See Supplemental Material at http://link.aps.org/supplemental/10.1103/PhysRevB.109.165411 for additional information about ARPES measurements, sample growth, electronic structure of CuTe using tunable laser-ARPES, temperature depen-

dence of the shadow band intensity, time, and energy resolution of the system and searching for CDW energy gap using laser ARPES, which also includes Refs. [35–37].

[35] H. Zhong, C. Bao, T. Lin, S. Zhou, and S. Zhou, Rev. Sci. Instrum. **93**, 113910 (2022).

[36] C. Bao, H. Zhong, S. Zhou, R. Feng, Y. Wang, and S. Zhou, Rev. Sci. Instrum. **93**, 013902 (2022).

[37] A. Fero, C. Smallwood, G. Affeldt, and A. Lanzara, J. Electron. Spectrosc. Relat. Phenom. **195**, 237 (2014).

[38] T. Sugimoto, D. Ootsuki, C. Morice, E. Artacho, S. S. Saxena, E. F. Schwier, M. Zheng, Y. Kojima, H. Iwasawa, K. Shimada *et al.*, Phys. Rev. B **92**, 041113(R) (2015).

[39] P. Chen, Y.-H. Chan, X.-Y. Fang, Y. Zhang, M.-Y. Chou, S.-K. Mo, Z. Hussain, A.-V. Fedorov, and T.-C. Chiang, Nat. Commun. **6**, 8943 (2015).

[40] Y. Wang, J. Ren, J. Li, Y. Wang, H. Peng, P. Yu, W. Duan, and S. Zhou, Phys. Rev. B **100**, 241404(R) (2019).

[41] H. Hedayat, C. J. Sayers, D. Bugini, C. Dallera, D. Wolverson, T. Batten, S. Karbassi, S. Friedemann, G. Cerullo, J. van Wezel *et al.*, Phys. Rev. Res. **1**, 023029 (2019).

[42] C. J. Sayers, H. Hedayat, A. Ceraso, F. Museur, M. Cattelan, L. S. Hart, L. S. Farrar, S. Dal Conte, G. Cerullo, C. Dallera *et al.*, Phys. Rev. B **102**, 161105(R) (2020).

[43] M. Obergfell and J. Demsar, Phys. Rev. Lett. **124**, 037401 (2020).

[44] A. A. Kolomenskii, R. Mueller, J. Wood, J. Strohaber, and H. A. Schuessler, Appl. Opt. **52**, 7352 (2013).

[45] P. Majchrzak, S. Pakdel, D. Biswas, A. J. H. Jones, K. Volckaert, I. Marković, F. Andreatta, R. Sankar, C. Jozwiak, E. Rotenberg *et al.*, Phys. Rev. B **103**, L241108 (2021).

[46] C. Bao, L. Luo, H. Zhang, S. Zhou, Z. Ren, and S. Zhou, Rev. Sci. Instrum. **92**, 033904 (2021).

[47] R. S. Li, L. Yue, Q. Wu, S. X. Xu, Q. M. Liu, Z. X. Wang, T. C. Hu, X. Y. Zhou, L. Y. Shi, S. J. Zhang *et al.*, Phys. Rev. B **105**, 115102 (2022).

[48] Y. H. Wang, D. Hsieh, E. J. Sie, H. Steinberg, D. R. Gardner, Y. S. Lee, P. Jarillo-Herrero, and N. Gedik, Phys. Rev. Lett. **109**, 127401 (2012).

[49] C. Bao, Q. Li, S. Xu, S. Zhou, X.-Y. Zeng, H. Zhong, Q. Gao, L. Luo, D. Sun, T.-L. Xia *et al.*, Nano Lett. **22**, 1138 (2022).

[50] H. E. Elsayed-Ali, T. B. Norris, M. A. Pessot, and G. A. Mourou, Phys. Rev. Lett. **58**, 1212 (1987).

[51] S. Kim, B. Kim, and K. Kim, Phys. Rev. B **100**, 054112 (2019).

[52] P. Cudazzo and L. Wirtz, Phys. Rev. B **104**, 125101 (2021).

[53] M. Campetella, G. Marini, J. S. Zhou, and M. Calandra, Phys. Rev. B **108**, 024304 (2023).

[54] C. N. Kuo, R. Y. Huang, Y. K. Kuo, and C. S. Lue, Phys. Rev. B **102**, 155137 (2020).

[55] L. Perfetti, P. A. Loukakos, M. Lisowski, U. Bovensiepen, H. Berger, S. Biermann, P. S. Cornaglia, A. Georges, and M. Wolf, Phys. Rev. Lett. **97**, 067402 (2006).

[56] C. Bao, H. Zhong, F. Wang, T. Lin, H. Zhang, Z. Sun, W. Duan, and S. Zhou, Phys. Rev. B **107**, L121103 (2023).